EPJ manuscript No.
(will be inserted by the editor)

Dissipative flows of 2D foams

Cantat I.[1] and Delannay R.[1]

[1] GMCM, Université de Rennes (CNRS), Campus de Beaulieu Bât. 11A CS 74205 263, av. du Général Leclerc 35042 Rennes Cedex, France

Received: date / Revised version: date

ccsd-00007608, version 1 - 21 Jul 2005

Abstract. We analyze the flow of a liquid foam between two plates separated by a gap of the order of the bubble size (2D foam). We concentrate on the salient features of the flow that are induced by the presence, in an otherwise monodisperse foam, of a single large bubble whose size is one order of magnitude larger than the average size. We describe a model suited for numerical simulations of flows of 2D foams made up of a large number of bubbles. The numerical results are successfully compared to analytical predictions based on scaling arguments and on continuum medium approximations. When the foam is pushed inside the cell at a controlled rate, two basically different regimes occur: a plug flow is observed at low flux whereas, above a threshold, the large bubble migrates faster than the mean flow. The detailed characterization of the relative velocity of the large bubble is the essential aim of the present paper. The relative velocity values, predicted both from numerical and from analytical calculations that are discussed here in great detail, are found to be in fair agreement with experimental results from [1].

PACS. 8 2.70.Rr, 83.50.Ha, 83.60.La

1 Introduction

Among complex fluids and structured materials, fluid foams, which are primarily materials of outstanding industrial importance, deserve too a particular attention as model systems. Indeed, they are governed by relatively well understood and simple local equilibrium properties. Further, each individual cell of a 2D foam can be followed during its motion and its deformation. The relation between the local structure and the induced macroscopic visco-elastic flow can thus be directly observed. These reasons explain why theoretical studies of 2D foam flows in viscous regimes are of growing importance [2,3,4,5,6,7,8,9].

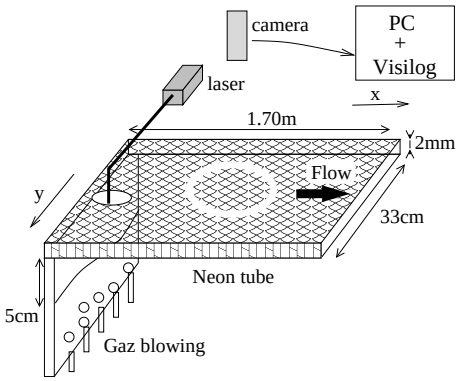


Fig. 1. *Schematic drawing of the set-up from which we collected the experimental results [1] referred to in the present theoretical paper.*

By a 2D foam, we refer here to foams confined between two horizontal plates and made up of a single bubble layer. The richness of the flow properties is largely related to the disorder of the foam structure [10], but we shall show in this paper that even few defects in an otherwise basically ordered structure may already induce strong modifications of the flow in a viscous regime.

If a constant foam flux is imposed in a Hele-Shaw cell (see Fig.1), a uniform pressure gradient is created between upstream and downstream to compensate the viscous drag on the plates. Lateral boundary effects are negligible and the reference flow at low velocity is thus a simple plug flow. At higher velocity, the plug flow becomes unstable for polydisperse foams. The velocity field, then dominated by the bubble size distribution and by its spatial correlations, leads to a very complex and fluctuating flow. Larger bubbles move faster than the smaller ones and the foam structure is fully reorganized with strong attractive correlations between bubbles of similar sizes. An understanding of this surprising foam behavior is out of reach without a satisfactory description of the underlying elementary instability which involves a single defect. Preliminary results on this instability were shortly discussed in a previous article [8], and experimental results are thoroughly described in [1]. In the following, we shall report in detail on theoretical and numerical investigations of the flow of a 2D monodisperse foam in which a single large bubble is embedded, leading to what is called hereafter the *large bubble instability*.

The viscous dissipation is localized on the Plateau borders touching the plates, *ie* the contact lines between the vertical foam films and the films wetting the plates. In a monodisperse foam which flows uniformly, viscous forces, averaged at the scale of few small bubbles, induce a uniform stress field oriented upstream. For a large bubble (denoted by LB in the following) the density of Plateau borders is smaller, and the averaged viscous stress is lower. The LB is, in a way, analogous to a low density drop embedded in a fluid submitted to a uniform gravity field. In both cases, the uniform stress field is balanced by a linear pressure field, and a resulting Archimedes-like force is exerted on the bubble (or respectively on the drop) in the direction opposite to that of the force field. This driving force, responsible for the LB migration, competes with the elastic reaction of the bubble network : a stable foam structure is obtained at low velocity. By contrast, the large bubble starts to migrate through the small bubble network, faster than the mean flow, when the foam velocity is large enough to induce a driving effect on the

large bubble greater larger than the plastic threshold of the foam (see Fig. 2).

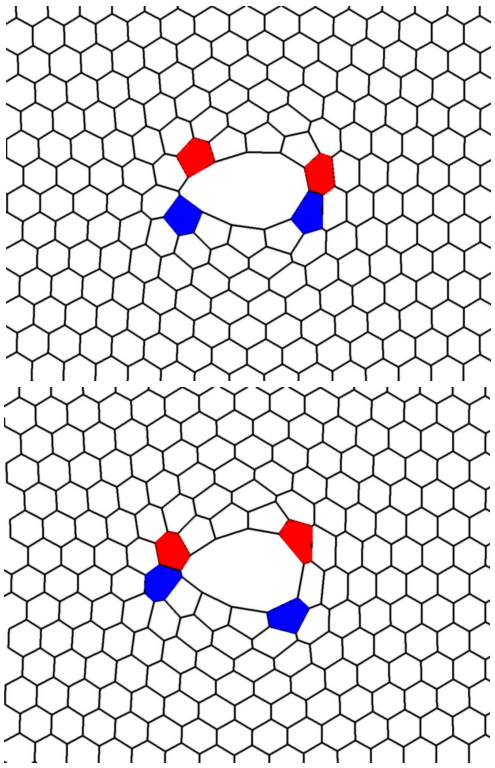


Fig. 2. *Two 'shots' of the LB migration through the foam, in the LB frame (numerical simulations). The foam crystalline orientation is the most favorable and the migration thus occurs in the same direction as the mean flow, to the right.*

Our main theoretical results consist of two scaling laws derived from general dimensional arguments for the velocity threshold (eq. 23) and for the large bubble velocity beyond that threshold (eq. 31). They are compared with the results of numerical simulations based on the vertex model [6] and with those of experiments presented in [1].

The paper is organized as follows. In Section 2, we discuss the main ingredients (bubble shape, viscous force, etc.) that play a role in the process by which the instability takes place. Section 3 presents a general frame, in which the foam is described by the positions of its vertices, that may be used for numerical simulations of any 2D foam flow. Section 4 is devoted to the qualitative description of the performed simulations and of the flow behavior so obtained. An analytical model, based on a continuous description, is introduced in Section 5, and allows quantitative comparison with the numerical results described in Section 6. The pressure field in the whole foam is discussed in Section 7. Finally, the results and perspectives are summarized in Section 8.

2 Specific properties of the 2D foam.

2.1 Equilibrium film shape.

The two-dimensional foam referred to here is a foam confined between to plates separated by a distance h, much smaller than the typical bubble size. For small values of h, the bubbles are organized in a single layer and every film touches the upper and the lower plates [11]. The Plateau borders touching the upper (or lower) plate draw a network Γ of connected curved lines, as shown on Fig.2. For 2D foams in equilibrium, the films separating two bubbles are part of vertical cylinders and the only non vanishing curvature is thus the constant curvature in a plane parallel to the plates, denoted by c_1 in the following. Thus Γ contains the whole information on the foam structure.

This property entails many important consequences specific to 2D foams in equilibrium [12] and yields a way of measuring the bubble pressure by simple image analysis using the Laplace relation $\Delta P = \gamma c_1$, where ΔP is the

pressure difference between two adjacent bubbles and γ the surface tension. In a flowing foam, the viscous forces, which are localized close to the plates, modify the contact angle θ as depicted on Fig.3 and 4. Both curvatures may be then of the same order of magnitude as evaluated in section 2.3 and the pressure can no more be read on a foam image, as the mean curvature is not measurable easily anymore.

2.2 Viscous forces.

The effective viscosity of a liquid foam pushed between two plates, *ie* the driving force to velocity ratio, is typically one or two orders of magnitude larger than that of the pure liquid phase, despite the very large amount of gas ($> 95\%$) trapped in the material [2,13,14,15]. This surprising behavior is due to the existence of very small length scales at which the liquid phase is confined in the structure. In the 2D geometry, the dominating process is the force between the Plateau borders and the plates. The viscous dissipation may have various origins, including the bulk viscosity of the liquid soap water, the viscosity of the surfactant monolayer and the diffusion resistance, leading to different relations between pressure drop and velocity [16,17]. Considering a fluid surfactant monolayer, we assume here that the dominating contribution comes from the bulk viscosity. The case of a rigid monolayer will nevertheless be considered too in section 6.2.

The local flow geometry close to the plates is very similar to the well-known Landau-Levitch situation, in which a plate is pulled out of a liquid [18,19]. The Plateau borders play here the role of the liquid reservoir and the relative motion between the liquid and the solid plate is due to the motion of the bubble walls. According to the Bretherton theory [20], the highest velocity gradients occur in a small domain connecting the Plateau borders and the wetting films, assumed to be at rest on each plate. This region is of characteristic thickness [20]

$$\delta(v) \sim R_{Pl}(\eta_w v/\gamma)^{2/3} \sim 5\,10^{-7} m \qquad (1)$$

with $\eta_w = 10^{-3} Pa\,s$ the liquid phase viscosity, $\gamma \sim 30\,10^{-3} N/m$ the surface tension, $v \sim 10^{-2} m/s$ the macroscopic velocity of the Plateau border and $R_{Pl} \sim 10^{-4} m$ the Plateau border size. The relevant Reynolds number for this problem is thus $Re = \rho\,\delta\,v/\eta_w \sim 5\,10^{-2}$, whose magnitude allows us to neglect the non-linear convective term in the Navier-Stokes equation. The viscous force $\boldsymbol{f}_v^0$ (per unit length of Plateau border) exerted on a Plateau border sliding at a velocity $\boldsymbol{v} = v\boldsymbol{u}_v$ on the plate varies nevertheless non linearly with v, namely as a power law with an exponent smaller than unity. It will be written $\boldsymbol{f}_v^0 = -\eta(v)\boldsymbol{v}$, $\eta(v)$ being an effective viscosity (with the dimension of a dynamic vioscosity). As the films swell when the foam velocity increases (see eq. 1), velocity variations occur on larger length scales and the effective viscosity decreases. We assume here that $\eta(v) \sim v^{-1/3}$ (Landau Levich exponent), although power laws with exponent values ranging between $-1/3$ and $-1/2$ are reported in the literature [17]. This force per unit length of Plateau border is finally of the order of $10^{-3} N/m$ and is expressed as [15] :

$$\boldsymbol{f}_v^0 = -\eta(v)\boldsymbol{v} = -\lambda\eta_w v Ca^{-1/3} |\boldsymbol{u}_v \cdot \boldsymbol{n}| \boldsymbol{u}_v; . \qquad (2)$$

with $Ca = \eta_w v/d$ the capillary number of the order of $3\,10^{-4}$. The numerical prefactor $\lambda \sim 10$ and the geometrical factor were measured in similar flow conditions, the latter involving $\boldsymbol{u}_v$ the unit vector of the film velocity direction and $\boldsymbol{n}$ the unit vector normal to the film (with an arbitrary orientation) [15]. The force direction is not clearly evidenced and seems difficult to determine directly. It is here assumed to be in the direction opposite to that of the film velocity.

It will be useful to express instead the viscous force per unit surface of the 2D foam averaged on the bubble scale (mean viscous stress on the plates). With a typical bubble size of $d \sim 10^{-2}m$ we obtain

$$\mathbf{F}_v = -\frac{\lambda \eta_w v}{d} Ca^{-1/3} \boldsymbol{u}_v \sim 10^{-1} N/m^2 \; . \qquad (3)$$

For comparison the viscous stress obtained for pure water with the same mean velocity is of the order of $\eta_w v/h \sim 10^{-2} N/m^2$.

2.3 Out of equilibrium film shape

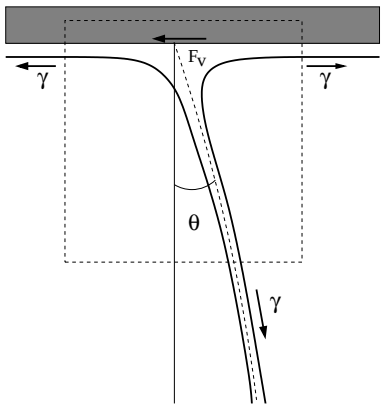


Fig. 3. *A schematic side view of the Plateau border during motion.*

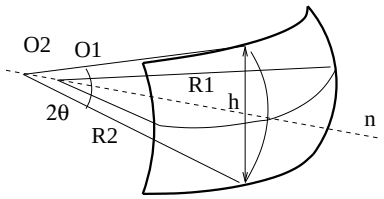


Fig. 4. *The film curvatures. The Plateau border curvature is locally $c_1 = 1/R_1$. In the plane normal to the plates and to the Plateau border the film section can be approximated by an arc of circle of radius R_2.*

During flow, as inertia and dissipation in the bubble walls are negligible, bubbles still obey the Laplace equation $\Delta P = \gamma c$ where c is the sum of the two main curvatures which remains constant on the whole bubble wall. The boundary conditions on the plates are modified by the viscous force, leading to another film shape. The force balance on an infinitesimal volume around a Plateau border (see Fig. 3) allows to determine the orientation θ of the fluid film at the contact with the wall,

$$\gamma \sin\theta = f_v^0 \; . \qquad (4)$$

The film shape is thus a surface of constant mean curvature with a contact angle at the plates depending on the local velocity. The two principal curvatures vary on the surface but may be approximated by $c_{p1} \sim c_1 = 1/R_1$ and $c_{p2} \sim c_2 = 1/R_2$, with c_1 the curvature in the symmetry plane between the two plates and $c_2 = 2\sin\theta/h \sim 30m^{-1}$ (see Fig. 4). Both curvatures may thus be of the same order of magnitude for centimeter-sized bubbles. As the mean curvature remains constant on a given film, if c_2 varies along the film, then c_1 varies too, and the Plateau border is no more an arc of circle.

3 Numerical simulation of a 2D flow

Simulations or analytical calculations make a compromise between the complexity of the dissipative function they use [2,3,5] and the number of bubbles they can consider [4,6,7,8,9]. The numerical model presented in this section is well adapted for a broad family of flow configurations in 2D. It is based on a realistic dynamical behavior, even at large velocities, and on a simplified foam structure description which allows to use a large number of bubbles at reasonable computational cost.

3.1 Numerical variables and equation of motion

As discussed above, the 3D film shapes are unknown. A local description of the 2D Plateau borders network Γ has been used by Kern et al. in numerical simulations performed with a small number of bubbles in which only c_1 is taken into account while c_2 [9] is neglected. This approach requires to discretize every Plateau border line and becomes very demanding for large scale simulations. For numerical efficiency, we choose to simplify the structure further by assuming vertical films to be planar, as already done in [6,8]. The Plateau borders touching the plates are straight lines (called edges), entirely determined by their end points (the vertices). Our numerical results have been quantitatively reproduced by Sanyal et al. with a method based on a Potts model [21].

The variables used are the vertex locations $\mathbf{r}_i$. The three edges which meet at a given vertex i have their end points located at $\mathbf{r}_i$ and $\mathbf{r}_j$ with $j \in J_i$. The system S_i is then defined as being composed of the vertex i with its three outgoing edges reduced by half, as depicted on Fig. 5. The equation of motion is provided by the force balance on each system S_i. The number of vertices remains constant as we forbid the occurrence of film breakage and of foam coarsening.

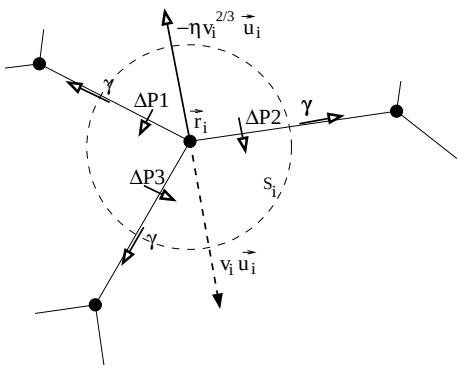


Fig. 5. *Force balance on the system S_i around the vertex i*

The tension force is, with $\mathbf{r}_{ij} = \mathbf{r}_i - \mathbf{r}_j$ and $r_{ij} = ||\mathbf{r}_i - \mathbf{r}_j||$,

$$\boldsymbol{F}_{t,i} = \gamma h \sum_{j \in J_i} \frac{\mathbf{r}_{ij}}{r_{ij}} \tag{5}$$

We define $\boldsymbol{n}_{ij}$ to be the normal to the edge (ij), oriented arbitrarily, say from a bubble A towards a bubble B, and $\delta P_{ij} (= P_B - P_A)$ to be the pressure jump on this edge. The resulting pressure force is then :

$$\boldsymbol{F}_{p,i} = -h \sum_{j \in J_i} \frac{r_{ij}}{2} \delta P_{ij} \boldsymbol{n}_{ij} \tag{6}$$

Finally the viscous force determination imposes some additional approximations. The whole system S_i is assumed to move with the same velocity as the vertex (i) : $\mathbf{v}_i = v_i \mathbf{u}_i$. Thus we get

$$\boldsymbol{F}_{v,i} = -k \sum_{j \in J_i} |\frac{1}{2}\mathbf{r}_{ij} \times \mathbf{u}_i| v_i^{2/3} \mathbf{u}_i \tag{7}$$

with the prefactor k obtained from eq. 3, $k = \lambda \eta_w^{2/3} \gamma^{1/3}$.

The equation of motion, $\boldsymbol{F}_{v,i} + \boldsymbol{F}_{t,i} + \boldsymbol{F}_{p,i} = 0$ imposes the orientation of $\boldsymbol{v}_i$ along the unit vector $\boldsymbol{F}_i/F_i$, with $\boldsymbol{F}_i = \boldsymbol{F}_{t,i} + \boldsymbol{F}_{p,i}$. We get thus the following explicit expression for the velocity, as a function of the positions $\boldsymbol{r}_j$, and of F_i which can itself be expressed as a function of the positions and the pressures (eq.5,6) :

$$\boldsymbol{v}_i = \boldsymbol{F}_i F_i^2 \left(k \sum_{j \in J_i} |\frac{1}{2}\mathbf{r}_{ij} \times \mathbf{F}_i| \right)^{-3/2} \tag{8}$$

As we will see now, the pressures are also related to the positions, so that the velocity is a function of the only variables $\boldsymbol{r}_j$. An iterative process is then possible as, for each time step, the velocities and consequently the displacements of the vertices can be computed, leading to an actualisation of their positions.

3.2 Explicit expression of the pressure

On the time scale of a few seconds considered in this paper, gas diffusion is negligible but pressure equilibrium is reached. The pressure is thus uniform in each bubble k and can be determined, under the assumption of an ideal gas, as a function of the area A_k of the bubble in contact with the plate, knowing the constant quantity of gas n_k trapped inside and its isothermal compressibility $\chi_T = 1/P_0$:

$$P_k = \frac{P^0 A_{k,0}}{A_k} \simeq P^0 - P^0 \, \frac{(A_k - A_{k,0})}{A_{k,0}} \, . \tag{9}$$

where

$$A_{k,0} = n_k R_{PG} T / h P^0 \tag{10}$$

is a reference value, obtained if the bubble pressure is equal to the global reference pressure P^0. This pressure is the same for every bubble in the foam, in contrast to the local reference P_{eq} that will be introduced in the following paragraphs. In our simulations, the reference pressure P^0 is strongly underestimated to enhance the numerical stability. Nevertheless, even if P^0 is smaller than its experimental value, it remains much larger than all the pressure variations induced by the flow and the system is in the incompressible limit (the relative variations of the bubble areas remain smaller than few %). The pressure field given by the product $P^0 \delta A/A$ is thus independent on P^0, even if both factors obviously depend on it. The choice of the compressibility value (or equivalently of the pressure reference) has therefore no real influence on the dynamical behavior, as checked numerically.

This formalism presents the big advantage to provide an explicit expression of the pressure as a function of the bubble geometry, in contrast to the classical Lagrange multiplier approach in which a strict incompressibility is assumed.

The reference area is chosen for each bubble as a fixed parameter. The actual area is computed after each displacement as a function of the positions of the vertices, assuming a polyhedral shape for the bubble. Finally, the pressure value in the bubble is deduced from eq. 9.

Note that the Plateau rules which constrain the values of the angles between the tangents of connected films at vertices, which are for instance equal to 120^o in a foam at equilibrium, are not imposed in this modeling because the films are represented by straight lines. In this case, the pressure difference between adjacent bubbles is no more

related to a film curvature but to a deviation of the angles from the reference value of 120^o.

3.3 Building of an initial foam structure

Periodic boundary conditions are imposed to the foam structure on the sides of the rectangular simulation box, the direction of the flow being parallel to the longer side. First of all, an artificial network of a few thousands of bubbles is built, with the positions and the connectivities of all vertices. Most results were obtained with an initial structure built from a perfect hexagonal network, but few simulations were performed with a disordered foam obtained from a Voronoi tessellation. Then a reference area is attributed to each bubble to reach the sought-after foam polydispersity and to create possibly very large bubbles in the foam. The system $\mathcal{S}_0$ is then relaxed to an equilibrium foam structure, using the iterative process detailed in paragraph 3.4 until the vertex motions become of the order of the numerical noise. After this first relaxation step, the areas are very close to the reference areas $A_{k,0}$.

3.4 Temporal evolution

The foam evolution is based on eq.8. It is determined iteratively in time from an initial structure $\mathcal{S}_0$, that may be either an equilibrium shape or an arbitrarily chosen out-of-equilibrium shape. Both transient or stationary processes may then be studied either in the presence of external perturbations or during relaxation to equilibrium. If we want to impose a flow in the direction x, we choose a set of vertices connected by a wiggly line $\mathcal{L}$ of edges whose average orientation is along y (Fig. 6). For that purpose, we select first a vertex with a first neighbor on the other side of the line $y = 0$. Then, from this point $\mathbf{r_i}$, we select the neighbor of smallest $|x|$ verifying $y > y_i$, and we iterate the process until we recover the initial point. The motion of the vertices which belong to that set $\mathcal{L}$ does not obey eq. 8 as do the other vertices, but they are forced to move at the desired velocity at each time step. This induces an artificial pressure discontinuity across the line $\mathcal{L}$, connecting the upstream and the downstream regions in the periodic box. The information propagates through the whole foam thanks to the pressure field.

The main algorithm is the following : During the time step dt, (a) the vertices belonging to $\mathcal{L}$ are displaced from $\mathbf{v}_0 dt$(in case of flow). (b) the bubble areas and pressures are updated. (c) Velocities, and thus displacements, are computed everywhere else with eq.8. (d) If the vertex displacements result in the formation of too small edges, T1 events are performed (see below), otherwise, (d') the displacements $\boldsymbol{v}dt$ are performed.

If an edge becomes smaller than a fixed value ϵ, a topological transformation T1 is performed, as explained on Fig. 7. For stability reasons, only one T1 is allowed to occur at each time step in the whole foam. In the rare case where two edges become simultaneously too small, we simply choose to perform only one of the two transformations, the other being done at the next time step. This would have to be improved to deal with different situations, for instance the case of foam shearing. The edge is switched

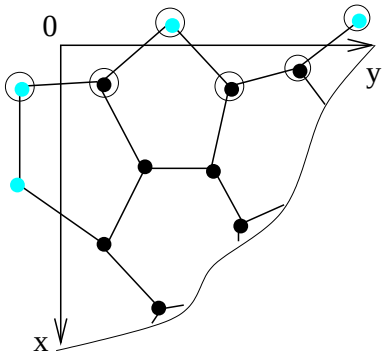


Fig. 6. *The encircled vertices belong to the line $\mathcal{L}$. Their velocities are fixed to a given value to impose the flow rate. The two axes are sides of the simulation box, gray vertices result from the use of periodic boundary conditions.*

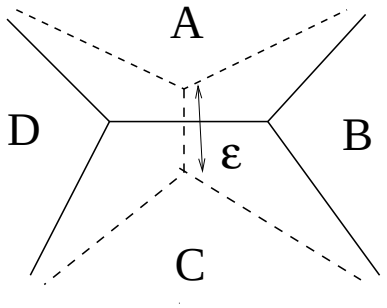


Fig. 7. *The structure before (dashed lines) and after (solid lines) a T1 transformation.*

perpendicularly to its previous orientation, and get a new length $\epsilon' \sim \epsilon$, which is an arbitrary constant parameter, and the connectivity of the four neighboring bubbles is modified. This transformation induces a concentration of tension forces around this new edge that leads to a rapid local relaxation governed by the same dynamical equations as the rest of the motion. As the process is very local, the 2D description presumably fails and the dissipation in the two vertical Plateau borders involved in the T1 must be of the order of the dissipation on the plates. This additional dissipation will be taken into account in a future modeling. In any case, if the characteristic time of a relaxation after a T1 remains small in comparison with the other time scales, they can be seen as instantaneous processes and their specific dissipation rates do not modify the foam behavior.

4 Large bubble instability : qualitative behavior

4.1 Performed simulations

We investigated the behavior of a monodisperse foam in which a single large bubble has been created. This defect is produced during the first relaxation step by imposing a large reference area to an arbitrary bubble chosen upstream, called LB. The results presented below were obtained with a LB area 20 times larger than the small bubbles area. The mean flow velocity is the control parameter of our study. Once the foam is equilibrated, the flow is turned on. The bubble areas adjust then slightly in order to establish the macroscopic pressure gradient between upstream and downstream. In the frame of the mean flow (in which $\mathcal{L}$ is at rest), a small upstream motion of the bubbles is then observed, corresponding to an area decrease upstream and an area increase downstream. Simultaneously, the foam deforms around the large bubble which tends to move faster than the mean flow. If the mean velocity is smaller than a threshold value, a stationary shape is obtained and the flow remains a plug flow. Otherwise, T1's occur around LB which begins to migrate.

The parameters ϵ, ϵ', $h\,P^0$, the box size and the time step were varied to test the numerical stability. The algo-

rithm becomes numerically unstable for a too large time step, whose maximal acceptable value is mainly related to $h\,P^0$ and to ϵ. The stability domain has not been systematically investigated, but we carefully checked the reproducibility of our results over a large range of parameters. Only ϵ has a noticeable influence on the threshold value as physically expected. It may indeed be seen as the characteristic size of a Plateau border, and is thus related to the liquid fraction ϕ of the foam by the relation

$$\phi \sim \epsilon^2 d/(hd^2) \sim \epsilon^2/(dh)\,, \tag{11}$$

with d the typical edge length, ϵ^2 the Plateau border section area and h the distance between the plates. Except for the results shown in Fig. 11, all results were obtained with a value of ϵ which corresponds to a liquid fraction of 0.5% (disregarding the additional water layer wetting the plates).

4.2 Disordered and ordered foams

In a monodisperse disordered foam, we don't observe a stationary motion of the large bubble for a velocity larger than the threshold. The shape of the large bubble, the magnitude and the direction of its relative velocity fluctuate strongly (Fig 8). When the large bubble moves at its highest velocity, its shape is elongated in the direction of its relative motion. The pinning of the large bubble by some defect in the disordered foam stops its migration. The bubble shape becomes then elongated in a direction perpendicular to that of the mean flow. Finally this shape destabilizes, by developing a tip downstream.

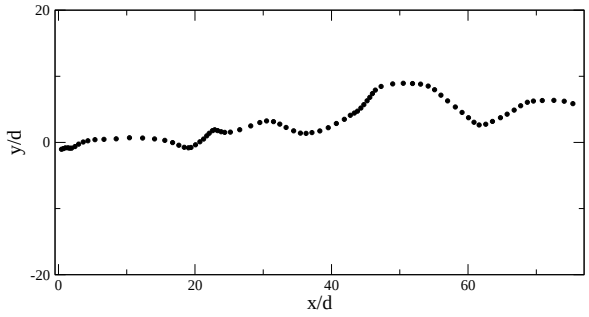


Fig. 8. *Trajectory of the large bubble center of mass in the mean flow frame in a case of a disordered foam (the flow is in the x direction). The distance between two successive points is proportional to its relative velocity.*

This tip grows by producing few T1's in the front of the large bubble and finally absorbs the full bubble and a new cycle begins. This qualitative behavior is in good agreement with experiments [1]. This jerky motion is puzzling and its extensive study is the aim of a future work. The explanation of the whole instability process requires first to understand the mean behavior of the large bubble. This is the aim of the present work.

The following results were thus obtained with an hexagonal network, only distorted by a single defect. A stationary regime, in which the large bubble moves at constant velocity, is reached after a very short transient. Despite the overall homogeneity of the foam, various kinds of motions may be observed with various stabilities and probabilities of occurrence. In the most frequent situation, the large bubble migrates solely thanks to T1's that take place near its front and its rear. The motion is periodic, and the

large bubble recovers exactly the same neighborhood after a migration of one bubble layer. Only few T1's, involving the first or second LB neighbors, are performed during this period. The crystalline organization is perfectly restored beyond the large bubble. The orientation of the relative LB motion may differ strongly from the direction of the mean flow. It occurs always along the most favorable crystalline direction (see Fig.2) and the angle between the mean flow and the relative velocity of the large bubble may thus reach 30^o.

More rarely, for slightly different initial conditions, a well defined wake may appear, with few bubbles moving behind the large bubble with the same velocity. This is observed in experimental flows too. Several choices seem thus to be offered to the large bubble, which may explain the large fluctuations observed experimentally and numerically in disordered foams.

Detailed numerical results found for the velocity threshold and the relative velocity of the large bubble are presented in the next section together with analytical predictions. They are obtained for LB trajectories in the direction of the flow, without wake, which is the most probable situation. The velocities, averaged over a set of experiments, are in fair agreement with predicted values as shown on Fig.14.

5 Continuous description

The numerical results are compared hereafter to analytical predictions based on a completely different point of view. We partially forget the specific foam structure, at least outside the large bubble, and we treat it as an elasto-plastic continuum medium. This point of view has already been successfully adopted by Kabla et al. in a quasi-static context [22]. Scaling behaviors are determined to emphasize the main physical processes involved, independently of any numerical prefactor. We give in the following subsections the analytical expressions of the various forces exerted on the network of small bubbles, per unit surface of foam (as seen from above), averaged over a few bubbles.

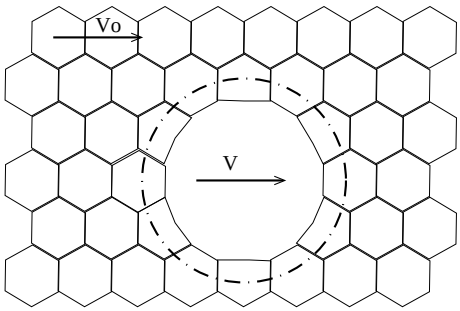


Fig. 9. *Internal system and external system, separated by the dashed circle.*

5.1 Viscous forces

Below the threshold, the viscous forces are well determined, as the velocity field is $\mathbf{v}(x, y) = v_0\mathbf{u}_x$ everywhere. The migration of the large bubble induces of course velocity variations in the foam, but the LB may move at high speed among the others with only very localized variations of vertices (and films) velocities. The migration occurs through a fracture process : few vertices at the front of the large bubble are accelerated until they reach their downstream neighbors and undergo a T1. Then the small bubbles initially in contact with these vertices move on the sides of LB and their vertices recover the mean velocity

v_0. The vertices between LB and their new downstream neighbors are then accelerated at their turn. A similar but inverted transformation occurs behind the large bubble. Thus velocities higher than v_0 and T1 transformations are confined in the internal system defined on Fig.9. In the external system, the variations of the network deformation due to the LB migration occur without topological rearrangements and induce only negligible velocity gradients.

For these reasons the velocity field is assumed to be $v_0\mathbf{u}_x$ in the whole external domain, even above the threshold. The viscous force per unit foam surface is thus (see eqs.2,3),

$$F_{visc} = -\frac{\eta(v_0)v_0}{d}\mathbf{u}_x = -\nabla\left(\frac{\eta(v_0)v_0 x}{d}\right) \qquad (12)$$

5.2 Pressure field

The pressure in a foam is heterogeneous, even at equilibrium. Its value is mainly related to the foam topology and to the number of sides n of each bubble and arise from the competition between tension forces which tend to shrink the bubbles and pressure forces which tend to inflate them. This effect remains present even when the foam flows and is then superimposed with purely dynamical pressure variations. To better evidence the dynamical contributions, we define the equilibrium part of the pressure in a given flowing structure as the pressure in each bubble after relaxation to the closest equilibrium shape. The latter shape is obtained numerically by fixing the line $\mathcal{L}$ of vertices and relaxing the rest of the foam. As the foam is only locally deformed, relaxation occurs usually, as desired, with no need of T1 transformation. This somewhat artificial splitting of the total pressure in two terms proved to be very powerful, as it allows us to reach a full and simple analytical description of the complex pressure field, in good agreement with the results of computer simulations. Hereafter, the equilibrium pressure defined in that way will thus be the local reference pressure, remembered to be specific to each bubble. Its value is discussed in detail in paragraph 7. Our method should however be improved to tackle more complex situations in which the system can only relax through many T1 transformations.

The resulting force per unit foam surface due to the heterogeneous gas pressure is consistently split into two terms, namely:

$$\mathbf{F}_p = \mathbf{F}_{p,eq} - h\nabla\bar{P}, \qquad (13)$$

The first term of the right-hand side is by definition obtained in a foam at equilibrium, as discussed above. It will play no role in the dynamics. The second term is not very sensitive to the local structure of the foam, and we assume that it is correctly described by the gradient of a smooth dynamical pressure field defined as $\bar{P} = P - P_{eq}$. This field will be derived in section 7.

5.3 Tension forces

Liquid foams have a rather simple behavior at small strain. A linear elastic response is obtained in this case with an elastic coefficient scaling as γ/d [23,24]. If the stress reaches a given threshold, equally of the order of γ/d, plastic deformation occurs (through T1's).

The distribution of surface forces, due to tension forces, is first decomposed in the same way as the pressure, leading to

$$\mathbf{F}_t = \mathbf{F}_{t,eq} + \bar{\mathbf{F}}_t \tag{14}$$

with $\mathbf{F}_{t,eq} = -\mathbf{F}_{p,eq}$.

Considering an elastic and incompressible response of the foam we get

$$\mathbf{F}_t = -\mathbf{F}_{p,eq} + \frac{\gamma h}{d}\nabla^2\mathbf{X} \, , \tag{15}$$

where X is the displacement vector from the closest equilibrium shape obtained after relaxing the foam as explained previously. The weak foam compressibility is disregarded.

6 Instability threshold and large bubble velocity

6.1 Driving force

Using the three force expressions eqs. 12,13,15 and neglecting any inertial term, we get the following equation for the external system,

$$-\nabla\left(\frac{\eta(v_0)v_0 x}{d} + h\bar{P}\right) + \frac{\gamma h}{d}\nabla^2\mathbf{X} = 0 \, . \tag{16}$$

The equation of incompressibility div X=0 and the boundary conditions must be added to eq. 16.

The internal system shape is approximated by a disc $\mathcal{D}$ of diameter D centered at the LB position. As it tends to migrate towards positive x, its displacement is $\delta\boldsymbol{u}_x$. The parameter δ remains undetermined at that point, it will be expressed explicitly in the next section. So we get, as first boundary condition for eq. 16, $\mathbf{X} = \delta\boldsymbol{u}_x$ on $\mathcal{D}$. In computer simulations, boundary effects on the cell sides are actually disregarded as the problem is solved with periodic boundary conditions. In contrast, in real experiments in a Hele-Shaw cell of width $2L$ there is a frictionless slip on the lateral smooth boundaries, leading to $X_y = 0$ and $\sigma_{xy} = 0$ where σ is the elastic stress tensor. Boundary conditions have only a logarithmic influence on the force fields near the large bubble, varying as $ln(D/L)$. They are difficult to determine analytically and are not relevant for our purpose. As an illustration, we nevertheless give here the asymptotic expression of the elastic force exerted on the large bubble with a third condition, $\mathbf{X} = 0$ on the lateral boundaries, well documented in the literature in the context of viscous hydrodynamics [25,26].

The large bubble motion is governed by the resulting force induced by the external pressure field and the elastic stress acting on the internal system. This force F_x, oriented along the mean flow for symmetry reasons is, noting $\mathcal{C}$ the boundary of the internal system and $\boldsymbol{n}$ its normal,

$$F_x = h\int_{\mathcal{C}} -\bar{P}n_x + \frac{\gamma}{d}\left(2\frac{\partial X_x}{\partial x}n_x + \left(\frac{\partial X_y}{\partial x} + \frac{\partial X_x}{\partial y}\right)n_y\right) dl \tag{17}$$

The analytical expression of this force has been obtained by analogy with the problem of an infinite cylinder pushed at constant velocity in a viscous fluid between two walls which is solved in the literature [25]. The identification of each variable is based on the similarity between the equations governing an elastic solid and a viscous fluid. As detailed in Appendix A it leads to

$$F_x = \frac{\eta(v_0)v_0 D^2}{d} - \frac{\gamma h}{d}\frac{4\pi\delta}{\ln(\frac{2L}{D}) - 0.91 + 0.43\,\frac{D^2}{L^2} + ...} \tag{18}$$

The first term, oriented downstream, is the driving force for the instability. It is a pressure contribution corresponding to the missing viscous forces in the large bubble. It is similar to an Archimedes force in which the homogeneous gravity field would be replaced by the homogeneous viscous force field $-\eta(v_0)v_0/d\boldsymbol{u}_x$. The resulting pressure force is proportional to the force field intensity times the area of the hole. The second contribution, oriented upstream, is the elastic response of the foam. As expected, it is proportional to the elastic coefficient γ/d and to δ. The denominator is an infinite sum expanded in the small parameter D/L. Its logarithmic dominating term is specific to the 2D case, in which elastic problems cannot be solved without boundary conditions at finite distance. This explicit analytical solution allows to quantify roughly the influence of the cell size. In any case, as other numerical prefactors will be disregarded in the following, we neglect this logarithmic dependence and we only checked that the denominator remains close to unity. The driving force expression used in the next subsection is thus

$$F_x = \frac{\eta(v_0)v_0D^2}{d} - \frac{\gamma h\delta}{d} \tag{19}$$

From this force, compared to the viscous force exerted on the large bubble itself, we determine the value of δ in the following.

6.2 Instability threshold

At small velocity, the elastic response of the foam compensates the driving force and the large bubble has the same velocity v_0 as the rest of the foam. The viscous force applied to the internal system, *ie* that due to the foam films around LB, is given by $D\eta(v_0)v_0$ (see eq.2). This leads to the following equation for δ, with the use of eq. 19:

$$\frac{\eta(v_0)v_0D^2}{d} - \frac{\gamma h\delta}{d} = D\eta(v_0)v_0 \ , \tag{20}$$

and, in the limit $D \gg d$,

$$\delta \simeq \frac{\eta(v_0)v_0D^2}{\gamma h} \tag{21}$$

The threshold is reached when the maximal stress in the foam reaches the yield stress γ/d. The largest elastic stresses are localized in front of the large bubble and just behind and their values are determined from dimensional arguments. As the elastic coefficient scales as γ/d, they scale as $\gamma\delta/(dL_{geo})$, where L_{geo} is a length related to the problem geometry. The box size appears only through logarithmic corrections. In a purely continuous medium description, the small bubble size scales out and thus $L_{geo} \sim D$, which is the value retained in the next part 6.3. Anyway, the discrete nature of the foam should probably be taken into account here. The small length scale d influences the radius of curvature of the LB in the region surrounding the fracture tip, and therefore the stress concentration. Both assumptions $L_{geo} = D$ or d are thus investigated below, as each might be valid in some domain which depends on the actual aspect ratio.

From this, we deduce the maximal value $\delta_{max} \sim L_{geo}$ and the velocity threshold v_{th}:

$$\eta(v_{th})v_{th} \sim \gamma\frac{hL_{geo}}{D^2} \tag{22}$$

Using $\eta(v_{th})v_{th} = \gamma(\eta_w v/\gamma)^\alpha$ (see eq. 2) we get, with the adimensional capillary number $Ca = \eta_w v/\gamma$,

$$Ca_{th} \sim \left(\frac{hL_{geo}}{D^2}\right)^{\frac{1}{\alpha}} \quad (23)$$

Depending on the value of L_{geo} and on the value of α (between 0.5 and 0.66 as discussed in section 2.2), the model predicts an exponent for D ranging between -1.5 and -4. The experimental value is of the order of -3.7, in a case where $\alpha = 0.5$ (see Fig.10, from [1]). The choice $L_{geo} = d$, which is thus in better agreement with the experiments than is $L_{geo} = D$, reinforces the importance of the discrete structure of the foam. New numerical simulations, especially with a large range of large bubble size, are nevertheless needed to be fully conclusive.

The liquid fraction plays an important role in the plastic threshold [23], and therefore influences the prefactor in eq.23. In our vertex model simulation, the liquid fraction is related to the minimal distance ϵ allowed between two vertices before a T1 occurs (see eq. 11). The variation of the threshold with this parameter is displayed on Fig. 11. All the simulation results presented on the other graphs were performed with a fixed ϵ value, as small as allowed by the numerical stability.

6.3 Large bubble relative velocity

For flow velocities larger than the threshold, plastic transformations occurs regularly around the large bubble which migrates through the foam with a velocity v(t). As these T1's are strongly localized around LB, they can be considered as discrete events relaxing suddenly the largest part

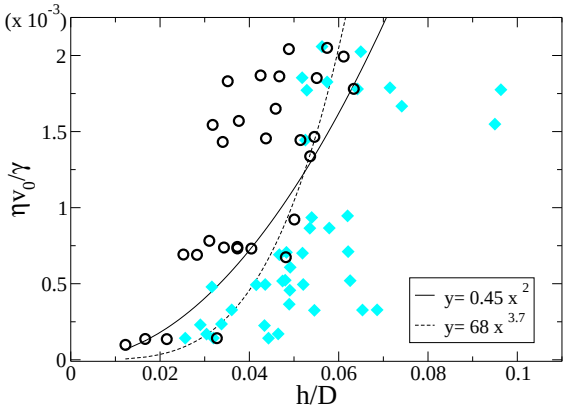


Fig. 10. *Experimental results from Cantat et al. [1]. Each point in the plane $(h/D; \eta v_0/\gamma)$ represents a flow, with a large bubble migrating (circle) or not (square). Two domains appear, separated by a boundary correctly fitted by the relation $Ca_{th} = 68(h/D)^{3.7}$ (dashed line). Fluctuations produce an overlap between the two domains which results in a large uncertainty on the exponent value. The boundary line, obtained from eq.23 with $L_{geo} = D$ and $1/\alpha = 2$ and an adjustable multiplicative prefactor, is further plotted (full line).*

of the elastic stress. Our model for the LB behavior is thus the following : if a T1 occurs at time $t = 0$, the elastic force vanishes, the value of δ is zero and the large bubble velocity is given by eq.20 : $\eta(v(0))v(0) = \eta(v_0)v_0 D/d$. Then δ increases with time, inducing an elastic stress increase and a LB velocity decrease. Finally δ reaches its limit D at $t = t_{max}$ and a new cycle begins (see Fig. 12).

As $\delta(t) = \int_0^t (v - v_0)dt$ the equation of motion becomes, between $t = 0$ and $t = t_{max}$, (see eq.20)

$$-\gamma h/d \int_0^t (v - v_0)dt + \frac{\eta(v_0)v_0 D^2}{d} = D\eta(v(t))v(t) \quad (24)$$

As detailed in Appendix B, this differential equation is analytically solvable. The approximate solution detailed

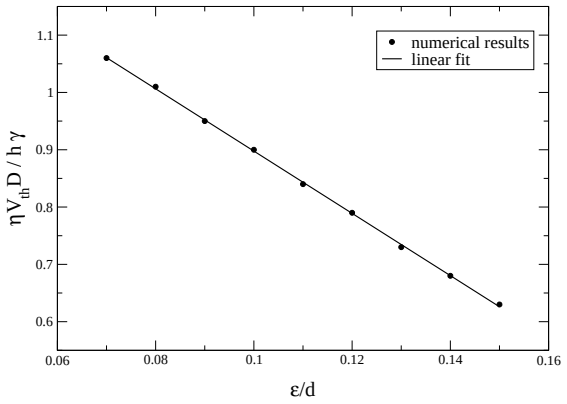


Fig. 11. *Velocity threshold as a function of the minimal distance ϵ allowed between two vertices before a T1 occurs.*

below is obtained by neglecting the variation of $\eta(v)$ with v. It differs only by few percents from the exact one and is much simpler (see Fig. 13). Taking the time derivative, we get

$$-\frac{\gamma h}{dD\eta}\left(v(t)-v_0\right)=\frac{dv}{dt} \tag{25}$$

$$v(t)=v_0+(v(0)-v_0)e^{-t/\tau} \tag{26}$$

$$\tau=\frac{d\,D\,\eta}{\gamma\,h} \tag{27}$$

Expression 26 is valid until δ reaches $\delta_{max}\sim D$ at time t_{max}.

$$\int_0^{t_{max}}(v(t)-v_0)dt=D=-\tau(v(0)-v_0)\left(e^{-t_{max}/\tau}-1\right) \tag{28}$$

So

$$t_{max}=-\tau\,ln\left(1-\frac{d}{\tau v_0}\right) \tag{29}$$

and finally, with <> denoting the average in time,

$$<v-v_0>=\frac{D}{t_{max}}=\frac{-D}{\tau ln\left(1-\frac{d}{\tau v_0}\right)} \tag{30}$$

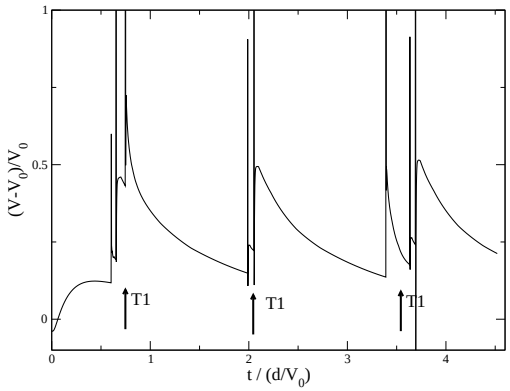


Fig. 12. *Numerical LB velocity as a function of time, for $v_0 > v_{th}$. T1's involving LB edges occur in avalanches of 2 or 3 events and are indicated by arrows. At these times the LB is suddenly deformed and the center of mass velocity diverges numerically. Just after a T1 avalanche, the elastic stress is strongly reduced and the LB velocity is large. As the stress accumulates in the small bubbles network the LB velocity decreases until the yield stress is reached and new plastic events occur. In contrast, if $v_0 < v_{th}$ the LB relative velocity tends to zero before the yield stress is reached.*

$$\frac{<v-v_0>}{v_0 D/d}=\frac{-v_{th}/v_0}{ln\left(1-\frac{v_{th}}{v_0}\right)} \tag{31}$$

The velocity threshold is consistently obtained from eq. 22 with $\eta=$ const., namely $v_{th}=\gamma h/\eta D$.

This expression is in good agreement with our numerical simulations (see Fig. 13). The small oscillations of the numerical points on both sides of the analytical curve are related to a bubble structure modification around LB at some velocities. The logarithmic behavior above the threshold renders the transition almost discontinuous. A small modification of the threshold value, due to a small polydispersity for example, induces a large variation of the LB velocity. The fluctuations observed experimentally

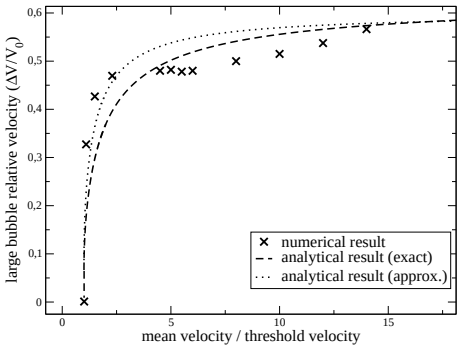


Fig. 13. *Large bubble relative velocity as a function of the mean flow velocity. The first analytical law is given by eq. 45 and the second one comes from eq. 31. Numerical prefactors are adjusted to obtain the best fit between numerical and analytical values. Their values are respectively 0.25 and 0.2, which is of the order of unity as expected. The ratio D/d is 3.*

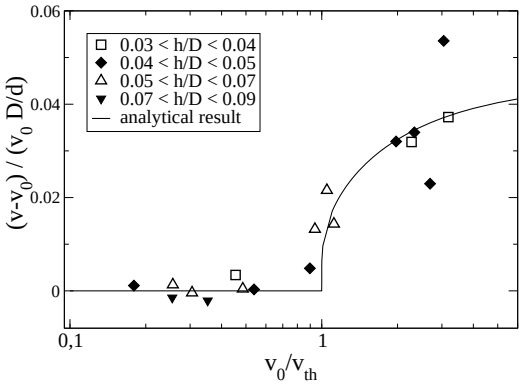


Fig. 14. *Experimental results from Cantat et al. [1]. Large bubble relative velocity as a function of the mean flow velocity, rescaled by the threshold velocity obtained on Fig.10, for various large bubble sizes. The analytical fit comes from eq. 31, with a single adjustable prefactor.*

are therefore relatively important, but the mean velocities, averaged over many experiments, are very well fitted by the previous law as shown on Fig.14, from Cantat and Delannay [1].

A better understanding of fluctuations is beyond the scope of this article. It would necessitate an improved description of the force field in the foam and of the structural disorder.

7 Pressure field.

7.1 Pressure at equilibrium

The pressure at equilibrium in a 2D foam obeys elegant and simple rules [12]. It is mainly related to the number of sides of each bubble. The average number of sides is six as a consequence of Euler's relation in 2D [12]. The pressure inside bubbles with $n > 6$ is larger than the external reference pressure whereas it is smaller when $n < 6$. When bubbles with $n \neq 6$ can be considered as relatively isolated defects in a monodisperse foam, the pressure distribution has been calculated by Graner et al. from an electrostatic analogy. Bubbles with $n \neq 6$ play the role of topological charges and modify the pressure field in the same way as positive or negative charges produce an electric potential. The induced pressure field around each defect is, with r the distance to the defect, (see [27])

$$P - P^0 = -\frac{\gamma}{d}\frac{(6-n)\pi}{3} ln(\frac{r}{d}) \qquad (32)$$

The logarithmic divergence is specific to the 2D geometry and we recover an expression similar to the electric potential produced by an infinite and uniformly charged line. The various contributions are additive, and a multipolar expansion can thus be used to derive the pressure field far from the defects. During its migration, the

large bubble adopts an elongated shape which is kept even after relaxation. The distribution of 5-sided bubbles on both sides of the large bubble with n_{LB} sides is equivalent to a quadrupolar distribution of topological charges, from which we deduce the dominant term in the pressure variation, up to a numerical prefactor,

$$(P - P^0) \sim n_{LB} d\gamma \left(\frac{2y^2}{(x^2+y^2)^2} - \frac{x^2}{(x^2+y^2)^2} \right) . \quad (33)$$

The results of numerical simulations are in good agreement with the predictions of eq. 33 as shown in figure Fig.15a-b.

7.2 Pressure during the flow

The pressure field in the flowing foam has already been discussed in detail in [8], and we just recall the main results here. As it is less sensitive to long range effects than the displacement field, it can be computed analytically without taking into account the positions of the boundaries. The final equation for the pressure is , with $\boldsymbol{r}_0$ the position of the large bubble,

$$\bar{P} = -\frac{\eta v_0 x}{d} + \frac{\eta v_0 D^2}{2\pi d} \frac{x - x_0}{(\mathbf{r} - \mathbf{r}_0)^2} , \quad (34)$$

The first term is the linear pressure variation responsible for the flow. The second term, compared to numerical results on Fig.16, is related to the foam deformation.

In contrast to the deformation of the foam and with the resulting tension forces, the pressure cannot be measured locally from images of a 2D foam. As shown on Fig. 16, it may nevertheless be very heterogeneous and plays a crucial role in the foam dynamics. It is thus an experimental challenge to determine the pressure in each bubble in a flowing foam.

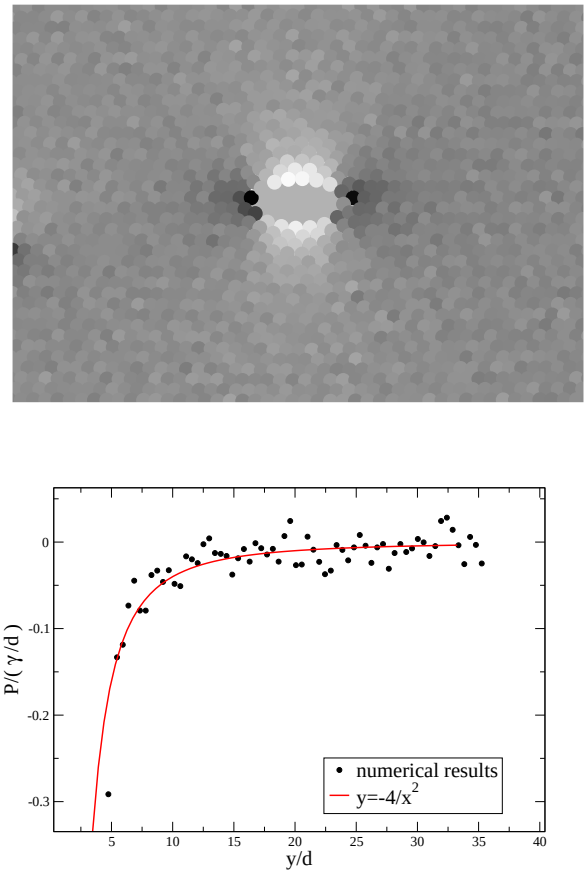


Fig. 15. *Pressure field around the large bubble, obtained by relaxation from an out of equilibrium situation, with a velocity larger than the threshold value. (a) Pressure field in gray level : pressure decreases from white to black (for clarity, the color of LB is arbitrarily chosen, its real pressure being lower than that of small bubbles). (b) Pressure along the horizontal segment $y = 0$ from LB to the right boundary. The solid line is a fit to the analytical expression given by eq.33, with an adjustable prefactor.*

The same approach can in principle be used to measure the displacement field. We thus compared the position of the bubble center before and after relaxation. The small

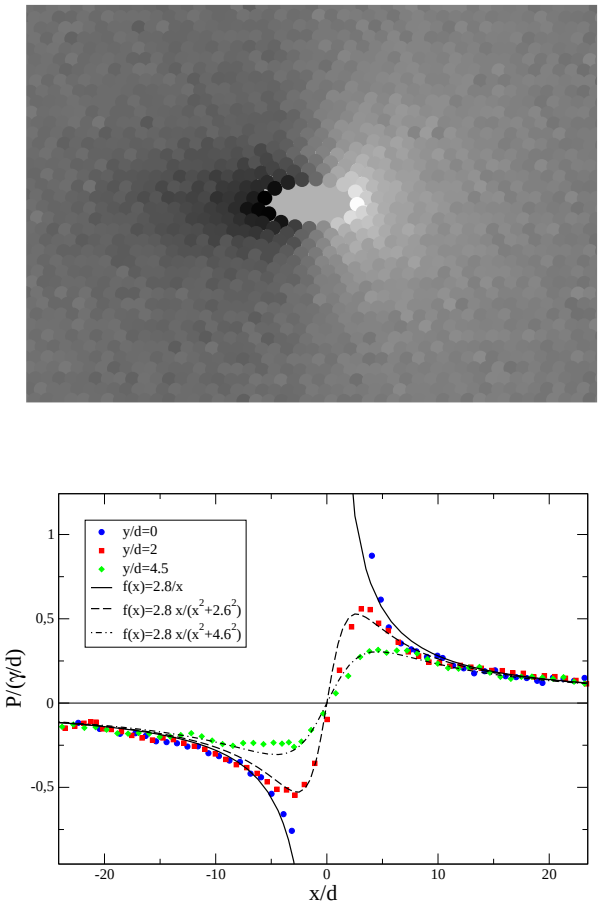


Fig. 16. *Pressure field in the foam after removing the equilibrium and linear contributions. The foam flows from the left* ($x < 0$) *to the right* ($x > 0$). *(a) Numerical results. Light gray corresponds to high pressure values. (b) Another view of the same results : pressure in the foam along the line* $y = const.$, *for three value of y. The line y=0 goes from upstream to downstream, trough the middle of LB. The values are well fitted by the analytical expression 34.*

compressibility of the foam induces a mean parabolic displacement of the form $X_x = \lambda(x^2 - L^2)$ because the bubble volumes increase upstream and decrease downstream during relaxation. Even with very small variations of bubble areas, as the displacement is the integral of the deformation, this effect is larger than the small elastic displacement we want to study. If this contribution is subtracted, the displacement field is nevertheless qualitatively different from the purely elastic displacement field computed with the software Freefem, for the boundary conditions obtained with the vertex model simulations. More simulations are needed to conclude to the physical relevance of such results and to exclude that they are just artefacts.

8 Summary and conclusion

In conclusion, we have shown that the *large bubble instability* can be reproduced with simple numerical simulations, keeping only the skeleton of the foam structure and the three key ingredients which are tension forces, viscous forces and volume conservation in the bubbles. The main physical aspects of this dynamical behavior is understood as a complex interplay between the viscous, elastic and plastic properties of the foam, seen as a continuum medium. This theoretical approach leads to a good agreement with numerical and experimental results. It can be adapted for various situations, as foam flows around obstacles for instance. Future work will have to take into account the disordered (or possibly crystallized) foam organization to deal with the velocity fluctuations of the large bubble.

A very important perspective is to predict the flow properties of a fully polydisperse foam. A mean field theory will probably be insufficient, as bubbles seem to be strongly coupled and as the flowing foam reorganizes itself with a resulting size segregation effect.

Acknowledgments: We thank *Rennes Métropole* and CNRS for financial support and G. Le Caër, J. Lambert, S. Cox, F. Graner and B. Dollet for enlightening discussions.

A Hydrodynamical analogy

Hydrodynamics equations for an incompressible viscous fluid of velocity v_h, pressure P_h and viscosity η is :

$$\eta \Delta \boldsymbol{v}_h - \nabla P_h = 0 \; ; \; \nabla \cdot \boldsymbol{v}_h = 0 \; . \tag{35}$$

The problem of an infinite cylinder of diameter D pushed at constant velocity V_h between two walls separated by a distance $2L$ has been solved by Faxen [25]. The variables can be identified as follows $\eta \mathbf{v}_h \leftrightarrow \gamma h/d \; \mathbf{X}$, $P_h \leftrightarrow \eta v_0 x/d + \bar{P}$ and $V_h \leftrightarrow \delta$. The expression of the force exerted on the cylinder is [25,26]

$$\begin{aligned} &\int_{\mathcal{C}} -P_h n_x + \eta \left(2\frac{\partial v_{hx}}{\partial x} n_x + \left(\frac{\partial v_{hy}}{\partial x} + \frac{\partial v_{hx}}{\partial y} \right) n_y \right) ds \\ &= -\frac{4\pi \eta V_h}{ln(\frac{2L}{D}) - 0.9157 + 1.73\,\frac{D^2}{(2L)^2} + ...} \end{aligned} \tag{36}$$

Using the variable identification, we obtain

$$\begin{aligned} &\int_{\mathcal{C}} -(\eta v_0 x/d + \bar{P}) n_x + \\ &\gamma h/d \left(2\frac{\partial X_x}{\partial x} n_x + \left(\frac{\partial X_y}{\partial x} + \frac{\partial X_x}{\partial y} \right) n_y \right) ds \\ &= -\frac{4\pi \, \gamma \, h \, \delta}{d \left(ln(\frac{2L}{D}) - 0.9 + 1.73\,\frac{D^2}{(2L)^2} + ... \right)} \end{aligned} \tag{37}$$

The term we need to compute is given by eq. 17 and is thus

$$F_x = \int_{\mathcal{C}} \frac{\eta v_0 x}{d} dx - \frac{4\pi \frac{\gamma h}{d} \delta}{ln(\frac{2L}{D}) - 0.9 + 1.73\,\frac{D^2}{(2L)^2} + ...} \tag{38}$$

B Resolution of eq. 24

Equation 24 is adimensional with the time unit $\tau = D\, d\, Ca_0^{2/3}/h v_0$. With, $\bar{t} = t/\tau$ and $\bar{v} = v/v_0$ and omitting the bar notation, we get,

$$\int_0^t (v-1) dt = \frac{D}{d} - \frac{3}{2} v^{2/3} \tag{39}$$

whose differentiation yields

$$v^{4/3} - v^{1/3} + \frac{dv}{dt} = 0 \tag{40}$$

The solution of this differential equation with separable variables is

$$t = H(v(t)) - H(v(0)) \tag{41}$$

with

$$H(x) = \ln \left(\frac{\sqrt{x^{2/3} + x^{1/3} + 1}}{x^{1/3} - 1} \right) - \sqrt{3} \tan^{-1} \left(\frac{2x^{1/3} + 1}{\sqrt{3}} \right) \tag{42}$$

The initial velocity is $v(0) = (D/d)^{3/2}$ and the maximum time before a T1 is given by

$$\int_0^{t_m} (v-1) dt = \frac{D}{d} - \frac{3}{2} v(t_m)^{2/3} = \frac{D}{v_0 \tau} \tag{43}$$

$$v(t_m) = \frac{2}{3} \left(\frac{D}{d} - \frac{D}{v_0 \tau} \right)^{3/2} \tag{44}$$

We finally express the mean relative velocity of the large bubble in terms of adimensional variables as:

$$< v - 1 > = \frac{D}{v_0 \tau} \frac{1}{H(v(t_m)) - H((D/d)^{3/2})} \tag{45}$$

References

1. I. Cantat and R. Delannay, preprint (2005).

2. L. W. Schwartz and H. M. Princen, J. Colloid Interface Sci. **118**, 201 (1987).
3. D. A. Reinelt and A. M. Kraynik, J. Colloid Interface Sci. **132**, 491 (1989).
4. J. A. Glazier and D. Weaire, J. Phys: Condens. Matter **4**, 1867 (1992).
5. X. Li, H. Zhou, and C. Pozrikidis, J. Fluid Mech. **286**, 379 (1995).
6. T. Okuzono and K. Kawasaki, Phys. Rev. E **51**, 1246 (1995).
7. D. J. Durian, Phys. Rev. Lett. **75**, 4780 (1995).
8. I. Cantat and R. Delannay, Phys. Rev. E **67**, 031501 (2003).
9. N. Kern, D. Weaire, A. Martin, S. Hutzler, and S. J. Cox, Phys. Rev. E **70**, 041411 (2004).
10. P. Sollich, F. Lequeux, P. Hébraud, and M. E. Cates, Phys. Rev. Lett. **78**, 2020 (1997).
11. S. Cox, D. Weaire, and M. F. Vaz, Eur. Phys. J. E **7**, 311 (2002).
12. D. Weaire and S. Hutzler, *The physics of foams* (University press, Oxford, 2000).
13. G. Hirasaki and J. B. Lawson, Soc. Pet. Eng. J. , p. 176 (1985).
14. Q. Xu and W. R. Rossen, Colloids and Surfaces A **216**, 175 (2003).
15. I. Cantat, N. Kern, and R. Delannay, Europhys. Lett. **65**, 726 (2004).
16. D. Buzza, C.-Y. Lu, and M. E. Cates, J. Phys. II (France) **5**, 37 (1995).
17. N. D. Denkov, V. Subramanian, D. Gurovich, and A. Lips, preprint (2005).
18. L. Landau and B. Levich, Acta Physicochim. USSR **17**, 42 (1942).
19. K. J. Mysels, K. Shinoda, and S. Frankel, *Soap films: Study of their thinning and a bibliography* (Pergamon, New-York, 1959).
20. F. P. Bretherton, J. Fluid Mech. **10**, 166 (1961).
21. S. Sanyal and J. A. Glazier, preprint (2005).
22. A. Kabla and G. Debregeas, Phys. Rev. Lett. **90**, 258303 (2003).
23. D. Weaire and M. A. Fortes, Adv. Phys. **43**, 685 (1994).
24. R. Höhler, S. Cohen-Addad, and H. Hoballah, Phys. Rev. Lett. **79**, 1154 (1997).
25. H. Faxen, 9e congrès des mathématiciens scandinaves, Helsigfors , 165 (1938).
26. J. Happel and H. Brenner, *Low Reynolds number hydrodynamics* (Martinus Nijhoff publisher, Dordrecht, 1986).
27. F. Graner, Y. Jiang., E. Janiaud, and C. Flament, Phys. Rev. E **63**, 011402 (2001).